Propagation of lower-band whistler-mode waves in the outer Van Allen belt: Systematic analysis of 11 years of multi-component data from the Cluster spacecraft

O. Santolík, E. Macusova, Ivana Kolmasova, Nicole Cornilleau-Wehrlin, Y. Conchy

AGU PUBLICATIONS

Geophysical Research Letters

RESEARCH LETTER
10.1002/2014GL059815

Key Points:
- Lower-band whistler-mode waves influence the outer radiation belt
- 11 years of wave propagation data from Cluster are analyzed by new methods
- Wave vector directions of intense waves are mostly field-aligned

Correspondence to:
O. Santolík,
os@ufa.cas.cz

Citation:
Santolík, O., E. Macúšová, I. Kolmašová, N. Cornilleau-Wehrlin, and Y. de Conchy (2014), Propagation of lower-band whistler-mode waves in the outer Van Allen belt: Systematic analysis of 11 years of multi-component data from the Cluster spacecraft, *Geophys. Res. Lett.*, *41*, 2729–2737, doi:10.1002/2014GL059815.

Received 4 MAR 2014
Accepted 1 APR 2014
Accepted article online 2 APR 2014
Published online 28 APR 2014

Propagation of lower-band whistler-mode waves in the outer Van Allen belt: Systematic analysis of 11 years of multi-component data from the Cluster spacecraft

Ondřej Santolík[1,2], Eva Macúšová[1], Ivana Kolmašová[1], Nicole Cornilleau-Wehrlin[3,4], and Yvonne de Conchy[4]

[1]Institute of Atmospheric Physics AS CR, Prague, Czech Republic, [2]Faculty of Mathematics and Physics, Charles University, Prague, Czech Republic, [3]LPP-CNRS-Ecole Polytechnique, Palaiseau, France, [4]LESIA-Observatoire de Meudon, Meudon, France

Abstract Lower-band whistler-mode emissions can influence the dynamics of the outer Van Allen radiation belts. We use 11 years of measurements of the STAFF-SA instruments onboard the four Cluster spacecraft to systematically build maps of wave propagation parameters as a function of position. We determine probability distributions of wave vector angle weighted by the wave intensity. The results show that wave vector directions of intense waves are close to a Gaussian-shaped peak centered on the local magnetic field line. The width of this peak is between 10 and 20 degrees. The cumulative percentage of oblique waves is below 10–15%. This result is especially significant for an important class of whistler-mode emissions of lower-band chorus at higher latitudes, well outside their source region, where a simple ray tracing model fails and another mechanism is necessary to keep the wave vectors close to the field-aligned direction.

1. Introduction

Electromagnetic whistler-mode waves in the Earth's magnetosphere significantly contribute to wave-particle interactions at different scales [e.g., *Tao et al.*, 2013, and references therein]. Especially, whistler-mode chorus has been shown to play an important role in the dynamics of the outer Van Allen radiation belt [*Thorne et al.*, 2013; *Miyoshi et al.*, 2013, and references therein]. Chorus is generated by nonlinear wave-particle interactions [e.g., *Katoh and Omura*, 2013] occurring close to the geomagnetic equator [*LeDocq et al.*, 1998; *Parrot et al.*, 2003a; *Santolík et al.*, 2005; *Li et al.*, 2013].

An important subclass of whistler-mode waves propagates in a frequency band below one half of the equatorial electron cyclotron frequency as lower-band chorus [*Katoh and Omura*, 2013; *Li et al.*, 2013]. Their importance has been demonstrated by their large averaged Poynting fluxes which have been found to be nearly 2 orders of magnitude larger than those for upper-band chorus waves [*Haque et al.*, 2010; *Santolík et al.*, 2010]. These waves are believed to contribute to the transfer of energy between different parts of the electron phase space distribution, and thus they not only influence losses of electrons from the radiation belts by their precipitation into the high-latitude ionosphere but also the acceleration of radiation belt electrons to relativistic energies [*Thorne et al.*, 2013]. Accurate description of propagation characteristics, on which all these interactions depend, is therefore important for successful modeling of the dynamics of the Van Allen radiation belts.

The assumption on propagation with wave vectors parallel to the background magnetic field is often made in theoretical studies of whistler-mode waves [e.g., *Katoh and Omura*, 2013] and in simulations of their interactions with radiation belts [*Tao et al.*, 2013]. The assumption of parallel propagation is compatible with many decades of ground-based chorus observations, with observations of reflected chorus by Cluster [*Parrot et al.*, 2003b], with statistical results based on measurements of whistler-mode waves by the THEMIS spacecraft close to the equatorial plane [*Li et al.*, 2013], and with a subset of whistler-mode chorus measurements of the Polar spacecraft [*Haque et al.*, 2010]. However, both these latter studies, as well as previous analysis of data from the Cluster spacecraft [e.g., *Santolík et al.*, 2009; *Agapitov et al.*, 2013], also find waves at high inclinations from the background field lines, close to the whistler-mode resonance cone.

In this letter, we address the following question: Do the lower-band whistler-mode emissions dominantly propagate with wave vectors parallel to the background magnetic field in the outer Van Allen belt? For our analysis, we use an unprecedented database of measurements of the STAFF-SA instruments onboard the Cluster spacecraft. We systematically determine the probability density functions of propagation characteristics of chorus, and we develop a new method to naturally weight the results by the intensity of observed waves. As the spacecraft orbits scan different regions of the Earth's magnetosphere, we build maps of wave propagation parameters in a wide range of magnetic latitudes.

2. Data Set

Our analysis is based on 11 years of measurements of the Cluster spacecraft constellation, between 1 January 2001 and 31 December 2011. We have used data collected by the STAFF-SA instruments onboard all four Cluster spacecraft [*Cornilleau-Wehrlin et al*., 2003]. These instruments analyze signals from three orthogonal magnetic antennas and two spin plane electric antennas. Onboard calculations result in multi-component spectra composed of spectral matrices collecting power spectral densities, mutual phases, and coherences of these signals. The analysis is done in 27 logarithmically spaced frequency channels covering the frequency range from 8 Hz to 4 kHz, with a time resolution of 4 s in the normal measurement mode. In the fast mode, data in a limited set of 18 frequency channels (frequency range from 60 Hz to 4 kHz) are obtained with a time resolution of 1 s. The STAFF-SA instruments were operational for 84% of time during the analyzed 11 year interval, of which approximately 3% were recorded in the fast measurement mode.

To construct our database, all collected data were first limited to the intervals of radial distances (R) between 2 and 11 R_E, and magnetic dipole latitudes (λ_m) between −60° and +60°. This limitation removed the orbital segments close to the spacecraft apogee and reduced the observational time down to 12%, corresponding to a total number of more than 42 million multi-component spectra. To facilitate the inclusion of our results into the radiation belt models, we have converted the position of each measurement into the L^* coordinate. We have obtained these values from the ONERA-DESP library [*Boscher et al*., 2008, now distributed as the International Radiation Belt Environment Modeling library] using the T89c model [*Tsyganenko*, 1989] with a real K_p input. Using the same model, we have also calculated the dipole latitudes λ_{m0} where the modulus of the static magnetic field is minimum along a given field line passing through the spacecraft position. The latitude λ_{m0} defines the modeled magnetic equator to which we will relate our results. A similar procedure has been previously used for the Polar chorus data set [*Santolík et al*., 2010]. Data for measurement intervals where the calculation of L^* or λ_{m0} was unsuccessful (typically, on open field lines) were excluded from the analysis. To avoid field lines with high-latitude minima of the magnetic field (occurring typically at high L^* on the dayside), we have additionally excluded all data points having λ_{m0} outside an interval of ±10° around the dipole equator. This procedure resulted in further reduction of the observational time down to an average total amount of more than 4100 h per spacecraft (4% temporal coverage of the total analyzed time interval) corresponding to 16 million multi-component spectra from all four spacecraft. This, nevertheless, represents the largest database of comprehensive wave observations in the inner magnetosphere that has ever been collected by a set of identical instruments. As the spacecraft orbits scan all the magnetic local times (MLT) every year, we obtain a homogeneous coverage of all the MLT sectors during the analyzed 11 year interval. The coverage of the different L^* and magnetic latitudes is given in Figure 1a. Our database allows us to characterize waves above $L^* \sim 2$ with an increasing latitudinal coverage, reaching ±45° at $L^* \sim 4$, and ±55° at $L^* \sim 6$.

To verify the assumptions about the wave polarization, we use a singular value decomposition (SVD) method [*Santolik et al*., 2003, equation (13)]. We analyze the 3D measurements of magnetic field fluctuations and at each analyzed frequency we obtain the ratio w_2/w_3 of the middle axis of the polarization ellipsoid to the largest one. The result is multiplied by −1 if the waves are left-hand polarized to obtain "ellipticity." Figure 1b shows the probability density function (PDF) calculated for all frequencies in separate bins of 0.1 L^* by counting the number of occurrences of ellipticity values in 64 elementary intervals, regularly distributed from −1 to +1, and by normalizing the PDF in each L^* bin to have a unity integral. The PDF in the ith elementary interval of a given L^* bin is therefore estimated as N_i/I, where N_i is the number of occurrences of ellipticity values in this interval, and $I = d\sum_{i=1}^{64} N_i$, d being the width of the elementary ellipticity interval. The

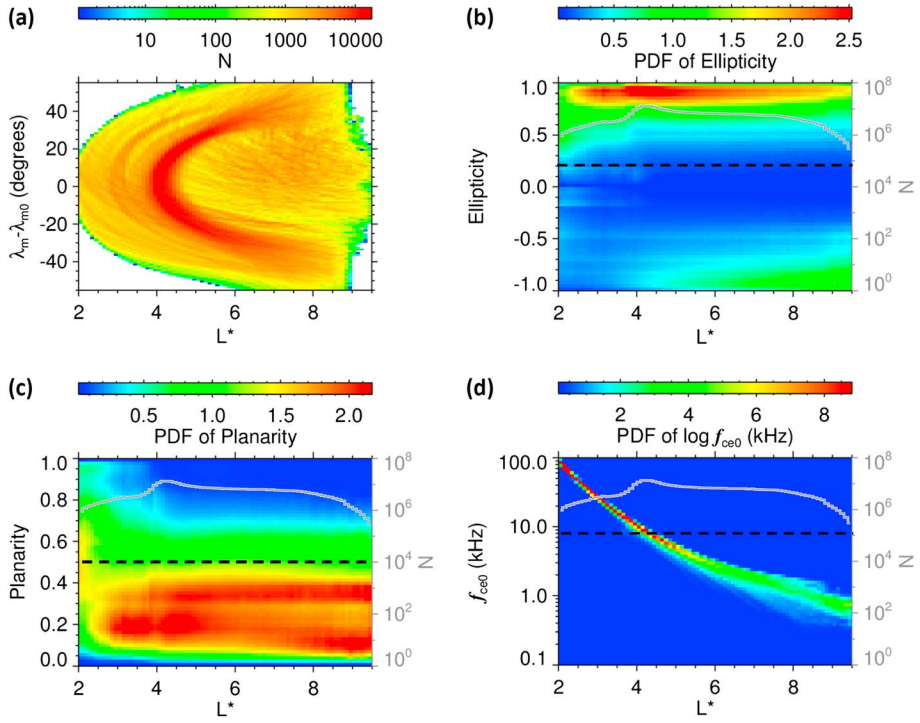

Figure 1. (a) Coverage of the inner magnetosphere by measurements of the Cluster mission represented by the number of multi-dimensional spectra collected in the bins of 0.1 L^* and 1° of magnetic latitude; (b–c) probability density functions of ellipticity and planarity from the singular value decomposition (SVD) analysis of magnetic spectral matrices (see text). The obtained values have been collected in 64 intervals and in bins of 0.1 L^* for $-55° < \lambda_m - \lambda_{m0} < 55°$. Thresholds of these parameters which are used in the analysis of wave vector directions are shown by the dashed lines; (d) probability density function of the common logarithm of the equatorial electron cyclotron frequency. The dashed line shows the limit of the STAFF-SA instrument for observing waves below 0.5 f_{ce0}. The number of individual spectral matrices in each L^* bin is given by a grey line with a scale on the right-hand side of Figures 1b–1d.

probability of obtaining an ellipticity value E contained in an arbitrary interval $E_1 < E \le E_2$ can be then calculated by integrating the PDF over this interval, from E_1 to E_2. The total number of individual spectral matrices in each L^* bin (given by the over-plotted grey solid line) is on the order of 10^6–10^7 and indicates a very high reliability of the obtained results. Most of the observed ellipticity values are close to +1 and correspond to the right-hand nearly circularly polarized waves consistent with propagation in the whistler mode. An ellipticity value of 0.2 is used for a lower threshold (shown by the dashed line) to exclude a fraction of linearly and left-hand polarized waves occurring especially at larger L^*.

Similarly, Figure 1c shows the "planarity" of magnetic field fluctuations calculated by the SVD method [*Santolik et al.*, 2003, equation (12)] as $1 - (w_1/w_3)^{1/2}$, where w_1/w_3 is the ratio of the smallest axis of the 3D polarization ellipsoid to the largest one. Plane waves have w_1 close to 0 and hence their planarity is close to 1. For isotropic noise and strongly non-planar waves, the polarization ellipsoid degenerates into a sphere and its planarity is low. To exclude these noisy spectral matrices from our analysis, we use a planarity threshold of 0.5 (dashed line) for all analyzed frequencies, corresponding to $w_1/w_3 < 0.25$. This threshold necessarily removes a substantial part of original data points (80%). The remaining spectral matrices can be analyzed to obtain the wave vector directions.

A natural definition of the frequency band for our analysis should reflect properties of the whistler-mode waves which change at one half of the electron cyclotron frequency. We therefore estimate the electron cyclotron frequency f_{ceM} in the anticipated source region at the magnetic equator for each data point. We obtain it, using the T89c model, from the minimum of the static magnetic field along a given field line passing through the spacecraft position. This value is corrected by a factor given by the ratio of the measured magnetic field strength B_0 at the spacecraft position and the T89c model field B_M at this position, $f_{ce0} = f_{ceM}\, B_0 / B_M$. The obtained values of f_{ce0} (Figure 1d) rapidly decrease with L^*, reaching 8 kHz around $L^* \sim 4$. Given the upper

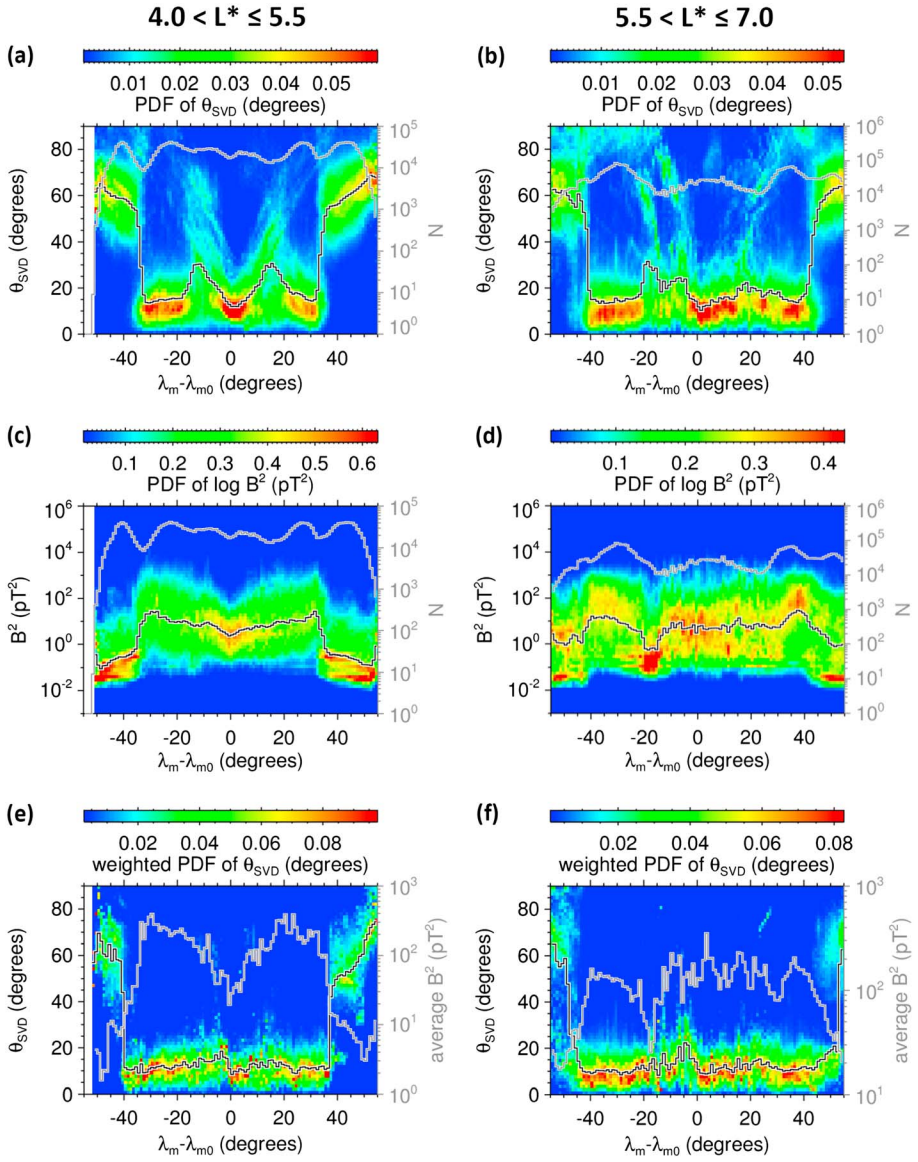

Figure 2. Analysis of wave propagation in the frequency band 0.1–0.5 f_{ce0} as a function of $\lambda_m - \lambda_{m0}$. Left-hand column: L^* from 4 to 5.5; right-hand column: L^* from 5.5 to 7. (a–b) Probability density function of the wave vector angle obtained by the SVD method using the magnetic spectral matrices; (c–d) probability density function of the common logarithm of the squared amplitudes of magnetic field fluctuations; median value in each λ_m bin is over-plotted by a black solid line in Figures 2a–2d; the number of individual spectral matrices in each λ_m bin is given by a grey line with a scale on the right-hand side of Figures 2a–2d; (e–f) weighted probability density function of the wave vector angle taking into account the squared magnetic field amplitudes; weighted median value in each λ_m bin is over-plotted by a black solid line; average squared magnetic field amplitude in each λ_m bin is given by a grey line with a scale on the right-hand side.

frequency limit of STAFF-SA instruments at 4 kHz, our database therefore allows us to analyze waves generated below 0.5 f_{ce0} for $L^* > 4$.

3. Results

Figure 2 shows properties of waves at frequencies between 0.1 and 0.5 f_{ce0}.The data are represented as a function of $\lambda_m - \lambda_{m0}$, in an interval of λ_m within ±55° from λ_{m0}, with 1° bins. After the reduction of the data set by the ellipticity and planarity thresholds and by using all suitable frequencies from each multi-component spectrum, we obtain reliable statistics based on 1.2 million of individual spectral matrices (10^3–10^5 in each

bin, see the grey line and right-hand scale of Figures 2a–2d). The left-hand column of Figure 2 shows results for an interval of L^* between 4 and 5.5. PDF of the angle θ between the wave vector, and the static magnetic field (Figure 2a) has been calculated by the SVD method [*Santolik et al.*, 2003, equation (9)] from the magnetic field measurements. Similarly to the preceding PDF calculations, we use 64 regularly distributed intervals of θ and normalization to the unity integral of the PDF. The results show that the propagation is predominantly at $\theta < 30°$, with an exception of high-latitude regions at $|\lambda_m - \lambda_{m0}| > 35°$ and a narrow low-latitude interval around $|\lambda_m - \lambda_{m0}| \sim 15°$ where some fraction of highly oblique θ values is obtained.

Figure 2c demonstrates, however, that the high-latitude regions generally contain waves with insignificant magnetic field power-spectral densities, close to the noise floor of the instrument which is between 10^{-4} and 10^{-3} pT^2 Hz^{-1} at analyzed frequencies between 0.1 and 0.5 f_{ce0}. The integral of these low power-spectral densities over the analyzed frequency interval gives the squared magnetic field amplitude around 10^{-1} pT^2, shown for high-latitudes in Figure 2c. For lower latitudes at $|\lambda_m - \lambda_{m0}| < 35°$, the squared amplitudes are higher, and the median value further increases by one order of magnitude with latitude from its minimum at λ_{m0}. The obtained PDF also shows a large spread of obtained values over two orders of magnitude, consistent with the "heavy-tail" log-normal distribution of the Poynting flux which was previously observed in the Polar data [*Santolík et al.*, 2010]. A question therefore arises if the obliquely propagating waves at $|\lambda_m - \lambda_{m0}| \sim 15°$ correspond to the intense part of the PDF of the squared amplitudes or if they are rather related to insignificant noise.

Taking into account the observed large variability of the magnetic field amplitudes, this question shows an important interpretation problem: both intense and weak waves are represented with the same weights in Figure 2a. Although unpolarized noise is implicitly suppressed by the planarity criterion in our analysis, very weak polarized waves and noise could still be able to strongly influence the results. In an attempt to resolve this problem, we have introduced a "weighted probability density function" (wPDF) in Figure 2e. Compared to the PDF which is estimated by counting the number of occurrences of obtained θ values in a set of 64 regularly distributed θ intervals, wPDF is estimated by calculating the sum of the simultaneously measured squared amplitudes corresponding to each of these θ intervals. The normalization is then again done separately in each of the 1° bins of $\lambda_m - \lambda_{m0}$, to obtain the unity integral of the wPDF. This normalization factor, divided by the number of measurements in each bin, gives the average squared amplitude (grey line and right-hand scale in Figure 2e). It again reflects the increase of wave intensity from the geomagnetic equator toward higher latitudes and then its decrease at $|\lambda_m - \lambda_{m0}| > 35°$. From the values of wPDF in Figure 2e, we have a very clear answer: the highly oblique θ values at $|\lambda_m - \lambda_{m0}| \sim 15°$ mainly corresponded to weak waves. Stronger waves, on the other hand, seem to prefer to propagate at $\theta < 30°$ in the entire interval of magnetic latitudes $|\lambda_m - \lambda_{m0}| < 40°$.

The right-hand column of Figure 2 shows the results of the same analysis as in the left-hand column but for a more distant zone of the outer Van Allen radiation belt, for L^* from 5.5 to 7. Compared to Figure 2c, the region of stronger waves in Figure 2d extends further out from the equator in both hemispheres, up to $|\lambda_m - \lambda_{m0}| > 40$–$45°$ and the wave intensity does not show a clear minimum at λ_{m0}. Otherwise, we obtain very similar behavior of PDFs and wPDFs of wave vector angles in Figures 2b and 2f, as in Figures 2a and 2e, respectively.

Both the above described PDF and wPDF estimates clearly show minima at very field-aligned wave vector angles below 5°. This reflects another important interpretation problem of our analysis: the probability to obtain θ in a narrow interval around its limiting value of 0° is approaching zero. This corresponds to the decreasing solid angle for regularly distributed θ intervals, or, in other words, to the Jacobian of the transformation between spherical and Cartesian systems. An integral of PDF over a given θ interval correctly gives the probability of occurrence. Similarly, an integral of wPDF over a given θ interval gives the fraction of the total magnetic field power (squared amplitude) which is contained in this interval, but an appropriate analysis should be done using $wPDF_\theta = wPDF / \sin\theta$. The integration over θ is then done with the corresponding Jacobian, obtaining the same results for the probability from $PDF / \sin\theta$ [*Li et al.*, 2013, equation (1)] or for the fraction of the total power-spectral density from $wPDF_\theta$.

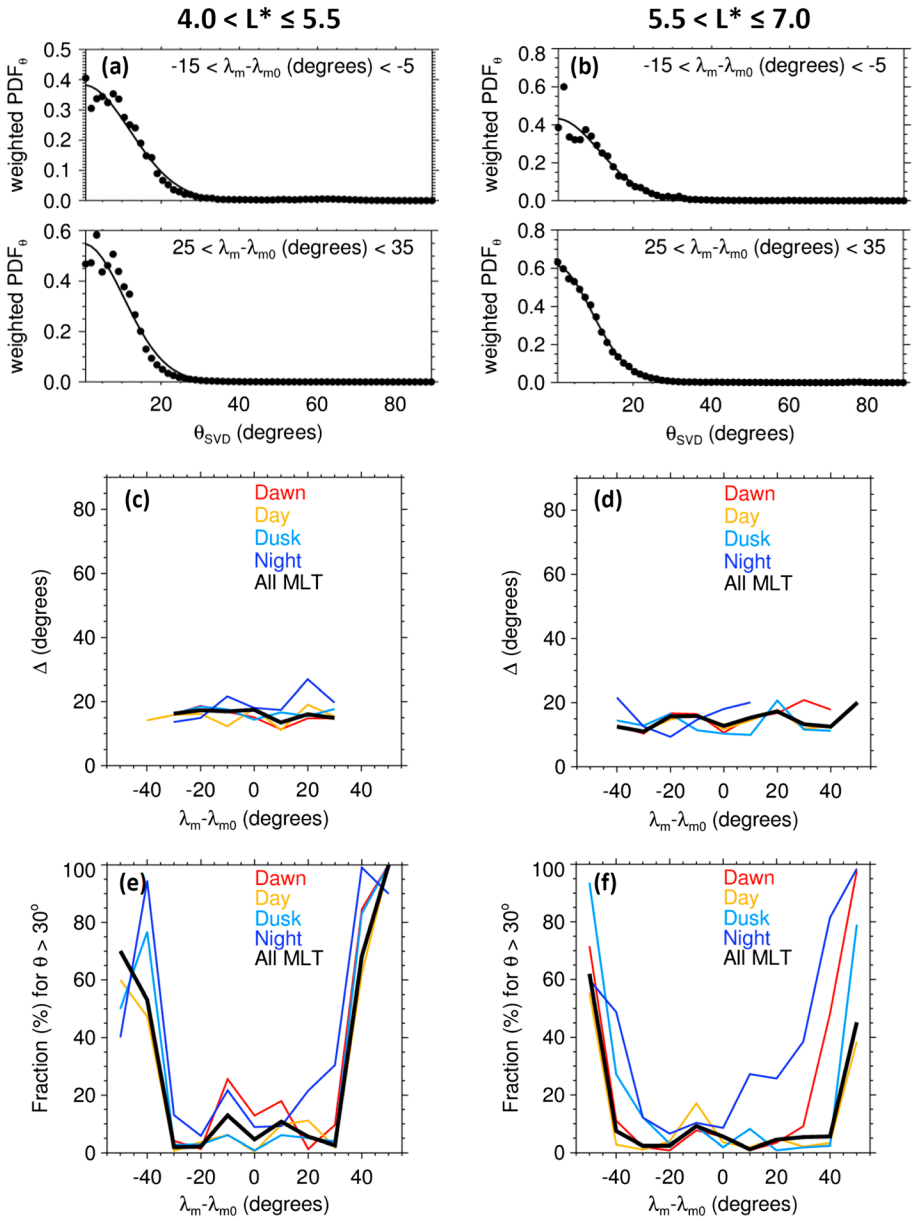

Figure 3. Parameters of the weighted probability density function of the wave vector angle normalized by sinθ. Left-hand column: L^* from 4 to 5.5; right-hand column: L^* from 5.5 to 7. (a–b) Weighted probability density function of the wave vector angle normalized by sinθ for two intervals of magnetic latitudes from $\lambda_{m0} - 35°$ to $\lambda_{m0} - 25°$, and from $\lambda_{m0} - 15°$ to $\lambda_{m0} - 5°$. A solid line shows a least-squares fit of a Gaussian model centered at the field-aligned direction. (c–d) Width Δ of a Gaussian model centered at the field-aligned direction; (e–f) fraction of the total magnetic power spectral density obtained for oblique waves at $\theta > 30°$; results for MLT between 0300 and 0900 are given by the red lines, yellow lines show results for 0900–1500 MLT, light blue lines for 1500–2100 MLT, dark blue lines for 2100–0300 MLT, and black lines show cumulative results for all MLT sectors.

When we transform the results in Figures 2e and 2f from wPDF to $wPDF_\theta$, we obviously obtain a stronger concentration of all the results near the field-aligned direction. Examples are, respectively, given in Figures 3a and 3b where we show $wPDF_\theta$ for two intervals of magnetic latitudes. The first of these intervals (from $\lambda_{m0} - 15°$ to $\lambda_{m0} - 5°$) corresponds to highly oblique θ values in Figures 2a–2b. The second example interval (from $\lambda_{m0} + 25°$ to $\lambda_{m0} + 35°$) contains the strongest emissions. A least-squares fit of a Gaussian model centered at the field-aligned direction, $wPDF_\theta = A \exp(-\theta^2 / \Delta^2)$, is shown by a solid line. The width Δ of this Gaussian model (Figures 3c and 3d) is usually found between 10° and 20° for convergent fits over the whole

range of magnetic latitudes. Slightly higher Δ values are obtained on the night side. Otherwise, we do not see significant differences of obtained Δ values in four different MLT sectors, nor in both analyzed intervals of L^*. Figures 3e and 3f show the fraction of the total magnetic power spectral density for oblique θ (from 30° to 90°), obtained as an integral of $wPDF_\theta$ in this θ interval. For the cumulative results for all MLT (black lines), the obtained oblique fraction is below 10–15%, confirming the predominantly field-aligned propagation. This fraction becomes higher for weak waves at high latitudes, with $|\lambda_m - \lambda_{m0}| > 35°$ in the near zone at $4 < L^* < 5.5$, and with $|\lambda_m - \lambda_{m0}| > 45°$ in the far zone at $5.5 < L^* < 7$. The results in four MLT sectors approximately follow this general trend, with an exception of the nightside and dawnside outer zones (shown, respectively, by blue and red lines in Figure 3f) where the oblique fraction dominates already for $\lambda_m - \lambda_{m0} > 30°$, or $\lambda_m - \lambda_{m0} > 40°$, respectively.

4. Discussion

We present new results on propagation of whistler-mode emissions in the outer Van Allen radiation belt using the largest database of multi-component measurements that has ever been collected from an identical set of instruments, covering one Solar cycle of operations of the Cluster spacecraft constellation. Its orbit allows us to scan a large range of latitudes outside the equatorial source region, unlike the THEMIS spacecraft which are orbiting close to the magnetic equatorial plane [*Li et al*., 2013]. We develop a method of weighting the obtained propagation characteristics by the observed intensity of the wave magnetic field in each predefined spatial bin. This is essentially the same process as the unavoidable and automatic weighting of different contributions to the spectral matrices which we use as the input of our analysis: different waves recorded during each individual analyzed time and frequency interval contribute to each individual magnetic spectral matrix with different weights proportional to their squared magnetic field amplitude.

Therefore, once the magnetic spectral matrices are used as an input for determining the wave vector directions, it is only logical to perform the same weighting also in the analyzed spatial and frequency bins. Besides this natural argument based on the analysis method, the weighting based on the squared magnetic field amplitude is linked to the purpose of investigating both linear and nonlinear interactions of chorus with electrons populations. These processes again mostly depend on the wave magnetic field amplitude [e.g., *Katoh and Omura*, 2013; *Tao et al*., 2013]. For example, the quasilinear diffusion coefficients are directly proportional to the squared magnetic field amplitude [*Thorne et al*., 2013, and references therein]. Obviously, other weighting methods can be used for other purposes, with consequences on the results. For example, weighting by the wave energy density or by the electric field amplitude would give more weight to oblique waves because the ratio of each of these quantities to the magnetic field amplitude increases with the wave vector angle. On the other hand, the group speed decreases with the wave vector angle and weighting by the Poynting flux leads to similar results as weighting by the squared magnetic field amplitude.

In the inner region $4 < L^* < 5.5$, we also observe a significant minimum of magnetic field amplitudes at the geomagnetic equator and their increase with the geomagnetic latitude in both hemispheres, up to 35° from the equatorial source region. A similar effect has been observed by *Haque et al*. [2012] who, using a much smaller data set, found an increase of Poynting fluxes of chorus with a minimum at the equator. Our results also clearly show that, at latitudes where we observe intense waves, the weighted distribution of wave vector directions of the lower-band whistler-mode emissions can be approximated by a Gaussian model with a width of 10–20°. This is consistent with the findings of *Haque et al*. [2010] who obtained lower time averaged Poynting fluxes for waves with highly inclined wave vectors. The conclusions of our study are different from those of *Agapitov et al*. [2013] who used a smaller subset of the Cluster database and found a rapid increase of the wave vector angle of the lower-band chorus with magnetic latitude. They used a different analysis method which was still based on magnetic spectral matrices but which did not take into account the lower intensities of waves with highly inclined wave vectors. They also used much more relaxed criteria for removing waves which do not satisfy the underlying approximation of a single right-hand polarized plane wave.

Our ellipticity criterion removes waves which do not correspond to the whistler mode. For this mode, the cold plasma theory [*Stix*, 1992] always gives the right-hand circular polarization of the magnetic field fluctuations in the plane perpendicular to the wave vector direction. The planarity criterion removes cases for which the wave vector direction cannot be reliably determined. These cases either correspond to

isotropic noise or to a wide distribution of waves with different wave vectors. For these latter cases, a method of wave distribution function [e.g., *Santolik and Parrot*, 2000, and references therein] would be appropriate. However, such a method would be hardly usable for a systematic statistical analysis based on large volumes of data. We therefore have to assume that the subset of data which satisfy the planarity criterion well represents the statistical properties of the whole data set.

Our results cannot be explained by a simple ray tracing theory which leads to a rapid increase of the wave vector angle of the lower-band chorus with magnetic latitude [*Chum and Santolik*, 2005]. A mechanism turning the wave vectors toward the field-aligned direction seems to be necessary to explain the observations in a broad interval of latitudes. One possibility would be that the waves are constantly generated at field-aligned wave vectors over the entire range of latitudes. This mechanism might correspond to the observed increase of wave amplitudes with latitude. However, this increase is only observed in the inner zone, and it might also correspond to the anticipated convergence of the wave ray traces propagating from the equator toward higher latitudes. The presence of plasma density ducts [*Bell et al*., 2009] can be one of the possible reasons for mostly field-aligned wave vector directions. Another mechanism for turning the wave vectors toward the field-aligned direction might be connected to non-linear scattering proposed by *Ganguli et al*. [2012].

The observations of mostly field-aligned wave vectors also substantiate our choice to characterize the analyzed frequency by the equatorial electron cyclotron frequency for a given magnetic field line. The rays of these waves would also be field aligned, and we therefore correctly characterize the frequency bands in the source region. We are, however, using averaged data and therefore we are unable to resolve if the waves included in our analysis are composed of structured whistler-mode chorus or shapeless hiss. This is an important aspect since nonlinear wave-particle interactions might depend on the particular time frequency structure of whistler-mode emissions. We have therefore started analysis of selected subsets of band-limited and structured whistler-mode emissions. The first results are similar to the results of the present letter. A detailed analysis of these data subsets is deferred to future studies.

Acknowledgments

We thank D. Boscher and his coworkers for maintaining the ONERA-DESP/IRBEM library that was used to calculate the L^* values, the model electron cyclotron frequencies f_{ceM}, and the latitude λ_{m0} defining the model magnetic equator. We acknowledge usage of the T89c model, with the Kp indices from http://swdcwww.kugi.kyoto-u.ac.jp/kp/. The data used to produce the results of this paper can be obtained from the ESA Cluster Science Archive. This work receives EU support through the FP7-Space grant agreement 284520 for the MAARBLE collaborative research project and from GACR grant 205-10-2279.

The Editor thanks Kristine Sigsbee and an anonymous reviewer for assistance in evaluating this manuscript.

References

Agapitov, O., A. Artemyev, V. Krasnoselskikh, Y. V. Khotyaintsev, D. Mourenas, H. Breuillard, M. Balikhin, and G. Rolland (2013), Statistics of whistler-mode waves in the outer radiation belt: Cluster STAFF-SA measurements, *J. Geophys. Res. Space Physics*, *118*, 3407–3420, doi:10.1002/jgra.50312.

Bell, T. F., U. S. Inan, N. Haque, and J. S. Pickett (2009), Source regions of banded chorus, *Geophys. Res. Lett.*, *36*, L11101, doi:10.1029/2009GL037629.

Boscher, D., S. Bourdarie, P. O'Brien, and T. Guild (2008), ONERA-DESP library V4.2, Toulouse, France, 2004–2008. [Available at http://craterre.onecert.fr/prbem/irbem/description.html.]

Chum, J., and O. Santolik (2005), Propagation of whistler-mode chorus to low altitudes: Divergent ray trajectories and ground accessibility, *Ann. Geophys.*, *23*, 3727–3738.

Cornilleau-Wehrlin, N., et al. (2003), First results obtained by the Cluster STAFF experiment, *Ann. Geophys.*, *21*, 437–456.

Ganguli, G., L. Rudakov, C. Crabtree, and M. Mithaiwala (2012), Multi-pass whistler gain in a magnetospheric cavity due to induced nonlinear scattering, *Geophys. Res. Lett.*, *39*, L16105, doi:10.1029/2012GL052942.

Haque, N., M. Spasojevic, O. Santolík, and U. S. Inan (2010), Wave normal angles of magnetospheric chorus emissions observed on the Polar spacecraft, *J. Geophys. Res.*, *115*, A00F07, doi:10.1029/2009JA014717.

Haque, N., U. S. Inan, T. F. Bell, and J. S. Pickett (2012), Spatial dependence of banded chorus intensity near the magnetic equator, *Geophys. Res. Lett.*, *39*, L17103, doi:10.1029/2012GL052929.

Katoh, Y., and Y. Omura (2013), Effect of the background magnetic field inhomogeneity on generation processes of whistler-mode chorus and broadband hiss-like emissions, *J. Geophys. Res. Space Physics*, *118*, 4189–4198, doi:10.1002/jgra.50395.

LeDocq, M. J., D. A. Gurnett, and G. B. Hospodarsky (1998), Chorus source locations from VLF Poynting flux measurements with the Polar spacecraft, *Geophys. Res. Lett.*, *25*, 4063–4066, doi:10.1029/1998GL900071.

Li, W., J. Bortnik, R. M. Thorne, C. M. Cully, L. Chen, V. Angelopoulos, Y. Nishimura, J. B. Tao, J. W. Bonnell, and O. LeContel (2013), Characteristics of the Poynting flux and wave normal vectors of whistler-mode waves observed on THEMIS, *J. Geophys. Res. Space Physic*, *118*, 1461–1471, doi:10.1002/jgra.50176.

Miyoshi, Y., R. Kataoka, Y. Kasahara, A. Kumamoto, T. Nagai, and M. F. Thomsen (2013), High-speed solar wind with southward interplanetary magnetic field causes relativistic electron flux enhancement of the outer radiation belt via enhanced condition of whistler waves, *Geophys. Res. Lett.*, *40*, 4520–4525, doi:10.1002/grl.50916.

Parrot, M., O. Santolik, N. Cornilleau-Wehrlin, M. Maksimovic, and C. Harvey (2003a), Source location of chorus emissions observed by cluster, *Ann. Geophys.*, *21*, 473–480.

Parrot, M., O. Santolik, N. Cornilleau-Wehrlin, M. Maksimovic, and C. Harvey (2003b), Magnetospherically reflected chorus waves revealed by ray tracing with cluster data, *Ann. Geophys.*, *21*, 1111–1120.

Santolik, O., and M. Parrot (2000), Application of wave distribution function methods to an ELF hiss event at high latitudes, *J. Geophys. Res.*, *105*, 18,885–18,894, doi:10.1029/2000JA900029.

Santolik, O., M. Parrot, and F. Lefeuvre (2003), Singular value decomposition methods for wave propagation analysis, *Radio Sci. 38*(1), 1010, doi:10.1029/2000RS002523.

Santolík, O., D. A. Gurnett, J. S. Pickett, M. Parrot, and N. Cornilleau-Wehrlin (2005), Central position of the source region of storm-time chorus, *Planet. Space Sci.*, *53*, 299–305, doi:10.1016/j.pss.2004.09.056.

Santolík, O., D. A. Gurnett, J. S. Pickett, J. Chum, and N. Cornilleau-Wehrlin (2009), Oblique propagation of whistler mode waves in the chorus source region, *J. Geophys. Res.*, *114*, A00F03, doi:10.1029/2009JA014586.

Santolík, O., J. S. Pickett, D. A. Gurnett, J. D. Menietti, B. T. Tsurutani, and O. Verkhoglyadova (2010), Survey of Poynting flux of whistler mode chorus in the outer zone, *J. Geophys. Res.*, *115*, A00F13, doi:10.1029/2009JA014925.

Stix, T. H. (1992), *Waves in Plasmas*, Am. Inst. of Physics, New York.

Tao, X., J. Bortnik, J. M. Albert, R. M. Thorne, and W. Li (2013), The importance of amplitude modulation in nonlinear interactions between electrons and large amplitude whistler waves, *J. Atmos. Sol. Terr. Phys.*, *99*, 67–72.

Thorne, R. M., et al. (2013), Rapid local acceleration of relativistic radiation-belt electrons by magnetospheric chorus, *Nature*, *504*, 411–414, doi:10.1038/nature12889.

Tsyganenko, N. A. (1989), A magnetospheric magnetic field model with a warped tail current sheet, *Planet. Space Sci.*, *37*, 5–20.